

# Learning entropy production via neural networks

Dong-Kyun Kim,<sup>1,\*</sup> Youngkyoung Bae,<sup>1,\*</sup> Sangyun Lee,<sup>1</sup> and Hawoong Jeong<sup>1,2,†</sup>

<sup>1</sup>*Department of Physics, Korea Advanced Institute of Science and Technology, Daejeon 34141, Korea*

<sup>2</sup>*Asia Pacific Center for Theoretical Physics, Pohang 37673, Korea*

## Abstract

This paper presents a neural estimator for entropy production, or NEEP, that estimates entropy production (EP) from trajectories without any prior knowledge of the system. For steady state, we rigorously prove that the estimator, which can be built up from different choices of deep neural networks, provides EP by optimizing the objective function proposed here. We verify the NEEP with stochastic processes such as those found in the bead-spring system and discrete flashing ratchet model. We also demonstrate that our method is applicable to high-dimensional data and non-Markovian systems.

---

\* These authors equally contributed to this work.

† hjeong@kaist.edu

Nonequilibrium states are ubiquitously observed from colloidal particles to biological systems [1–4]. Injection of energy, lack of relaxation time, or broken detailed balance are ordinary sources of nonequilibrium, and in general, such systems are in contact with a heat bath such as a fluid. Thus, to describe the behavior of a nonequilibrium system, it is necessary to investigate the energetics of the system [5]; however, experimentally, heat flow is difficult to measure directly [6–9]. In this case, measuring the entropy production (EP) can be one remedy to estimate heat flow in a nonequilibrium system.

Many techniques have been developed to accurately measure EP, such as approaches calculating irreversible currents [10]. These methods require detailed information from a governing equation though, so to address this issue, a few methods to estimate the EP rate without any prior knowledge of the system have been proposed, including the plug-in method [11], the Ziv–Merhav estimator [12–14], and the thermodynamic uncertainty relation (TUR) based estimator [10, 15, 16]. The plug-in and Ziv–Merhav methods estimate the EP rate through the Kullback–Leibler divergence [17], but they are only applicable for discrete state variables. Although the TUR-based approach suggests a framework for continuous variables through coarse-graining, it only provides the lower bound of the EP rate. Therefore, measuring the EP rate for continuous variables is still an open problem.

Various fields in physics have been employing machine learning (ML) to solve a wide range of non-trivial problems such as identifying relevant variables [18–20], identifying phase transitions [21–26], quantum many-body problems [27–34], and others [35]. While ML has also been applied to EP rate estimation [16], only the lower bound of the EP rate is given. Relatedly, in the ML community, a recent work by Rahaman et al. [36] proposed a neural network to measure an entropy-like quantity by unsupervised learning; however, the quantity was not physically well defined, i.e. it had no scale. To the best of our knowledge, estimating EP using neural networks has yet to be explored.

In this paper, we propose a neural estimator for entropy production (NEEP), which can estimate EP without any prior knowledge of the system. For Markov chain trajectory  $s_1, s_2, \dots, s_L$ , we build a function  $h_\theta$  that takes two states,  $s_t$  and  $s_{t+1}$ , where  $\theta$  denotes trainable neural network parameters. As shown in Fig. 1(a), the output of NEEP is defined as

$$\Delta S_\theta(s_t, s_{t+1}) \equiv h_\theta(s_t, s_{t+1}) - h_\theta(s_{t+1}, s_t). \quad (1)$$

Here,  $\Delta S_\theta(s_t, s_{t+1})$  satisfies the antisymmetric relation  $\Delta S_\theta(s_t, s_{t+1}) = -\Delta S_\theta(s_{t+1}, s_t)$ . We define the objective function to be maximized as

$$J(\theta) = \mathbb{E}_t \mathbb{E}_{s_t \rightarrow s_{t+1}} [\Delta S_\theta(s_t, s_{t+1}) - e^{-\Delta S_\theta(s_t, s_{t+1})}], \quad (2)$$

where  $\mathbb{E}_t$  denotes the expectation over  $t$ , which is uniformly sampled from  $\{1, \dots, L-1\}$ , and  $\mathbb{E}_{s_t \rightarrow s_{t+1}}$  is the expectation over transition  $s_t \rightarrow s_{t+1}$ . If detailed balance is satisfied, then the transition  $s \rightarrow s'$  and its reverse transition  $s' \rightarrow s$  equally appear in the ensemble of the trajectories. In this case, the optimized  $\Delta S_\theta$  is zero for all possible transitions, but if detailed balance is broken, then  $\Delta S_\theta$  becomes larger due to more irreversible transitions. In steady state,  $J(\theta)$  can be written as

$$J[h] = \sum_{i,j} p_i T_{ij} [(h_{ij} - h_{ji}) - e^{-(h_{ij} - h_{ji})}] \quad (3)$$

where we set  $h_{ij} \equiv h(s_i, s_j)$  and  $p_i \equiv p(s_i)$  for brevity, and  $T_{ji} \equiv p(s_i, t+1 | s_j, t)$  is a propagator. Because the neural networks tune output  $h_{\alpha\beta} \equiv h(s_\alpha, s_\beta)$  by optimizing  $\theta$ , the maximum condition for Eq. (3) becomes

$$\begin{aligned} 0 &= \partial_{h_{\alpha\beta}} J[h] \\ &= \sum_{i,j} [p_i T_{ij} (1 + e^{-(h_{ij} - h_{ji})}) (\delta_{i\alpha} \delta_{j\beta} - \delta_{i\beta} \delta_{j\alpha})] \\ &= p_\alpha T_{\alpha\beta} (1 - e^{(h_{\alpha\beta} - h_{\beta\alpha})}) - p_\beta T_{\beta\alpha} (1 - e^{(h_{\beta\alpha} - h_{\alpha\beta})}). \end{aligned} \quad (4)$$

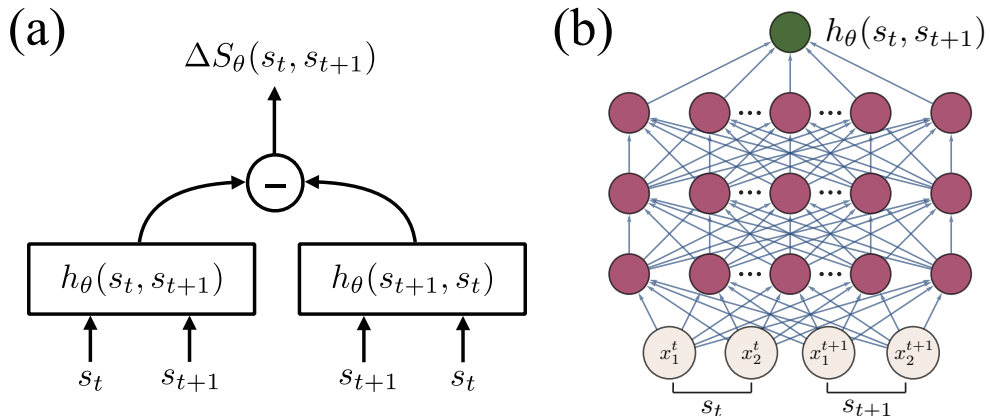


FIG. 1. (a) Architecture of the neural estimator for entropy production (NEEP). (b) Illustration of a multilayer perceptron (MLP) with three hidden layers for a  $N = 2$  bead-spring model where  $s_t = (x_1^t, x_2^t)$ .

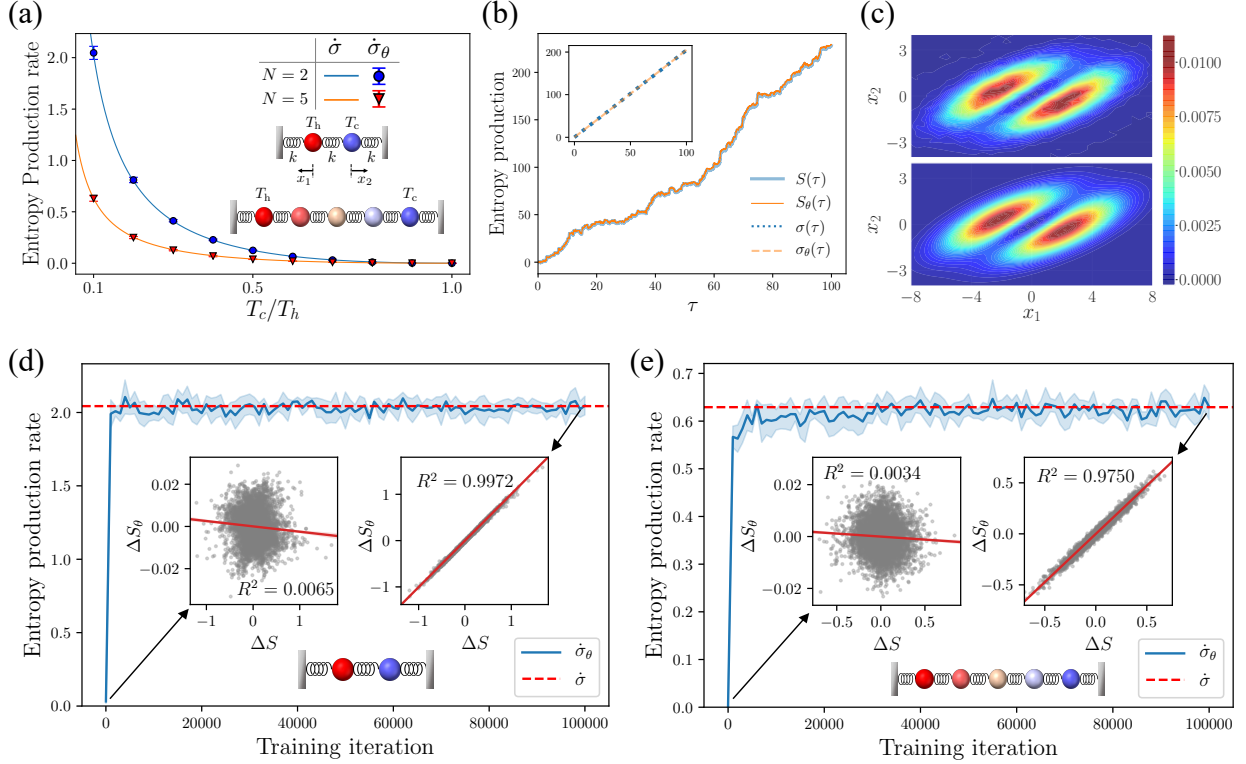


FIG. 2. (a) Entropy production rate as a function of  $T_c/T_h$  for models with two and five beads. The solid lines and symbols indicate the analytical and estimated values, respectively. (b) Cumulative EP over time  $\tau$  along a single trajectory, which is randomly sampled from the test set. The inset shows the ensemble averaged EP. (c) Local EP rate as a function of  $x_1$  and  $x_2$ . The top and bottom panels show the NEEP and the analytical results, respectively. (d,e) Estimated EP rate with respect to training iteration for (d) two beads and (e) five beads. The insets show scatter plots between estimated and true EP with a fitted linear regression line (solid red line). Error bars and shaded areas represent the standard deviation of estimations from five independently trained estimators.

Then the solution for the optimization problem is

$$h_{\alpha\beta} - h_{\beta\alpha} = -\ln(p_\beta T_{\beta\alpha}/p_\alpha T_{\alpha\beta}), \quad (5)$$

which is the definition of total entropy production [37] when  $T_{ji} = \tilde{T}_{ij}$ . Here,  $\tilde{T}_{ij}$  is the time-reversal propagator of  $T_{ij}$ . This proof supports the ability of our NEEP to learn appropriate EP. We maximize Eq. (2) via the stochastic gradient ascent method that is widely used in deep learning literature [38, 39]. See Supplemental Material I for training details.

To validate our approach, we estimate the EP of two widely studied nonequilibrium

systems: the bead-spring model for continuous state variables [1, 10, 40, 41] and the discrete flashing ratchet model for discrete state variables [13, 14, 42]. In addition, as more challenging problems, we apply NEEP to a high-dimensional continuous model and a non-Markovian model.

In the bead-spring model,  $N$  beads are coupled to the nearest beads or boundary walls by springs, and contacted with thermal heat baths at different temperatures, as described in Fig. 2(a). For displacements  $x_1, x_2, \dots, x_N$ , the dynamics of  $N$ -beads is governed by an overdamped Langevin equation

$$\dot{x}_i(\tau) = A_{ij}x_j(\tau) + \sqrt{2T_i/\gamma}\xi_i(\tau), \quad (6)$$

where

$$A_{ij} = -\frac{2k}{\gamma} \delta_{i,j} + \frac{k}{\gamma} (\delta_{i,j+1} + \delta_{i+1,j}). \quad (7)$$

Here,  $k$  is a spring constant,  $\gamma$  is the Stokes friction coefficient, and the temperature  $T_i$  of each heat bath linearly varies from  $T_c$  to  $T_h$ .  $\xi_i$  is an independent Gaussian white noise satisfying  $\mathbb{E}[\xi_i(\tau)\xi_j(\tau')] = \delta_{ij}\delta(\tau-\tau')$  where  $\mathbb{E}$  denotes the ensemble average. We set all the parameters to be dimensionless. For brevity, we set  $k_B = k = \gamma = 1$ . The linearly varying temperature induces thermodynamic forces which drive the system to a nonequilibrium state.

To attempt EP estimation in systems with continuous variables, we consider an  $N = 2$  bead-spring model, and as a further challenge, we also test with  $N = 5$  for high-dimensional continuous variables. Here,  $\dot{\sigma}$  is the analytical value of the ensemble averaged EP rate; Fig. 2(a) plots  $\dot{\sigma}$  for  $N = 2$  (5) with a blue (orange) solid line.

As illustrated in Fig. 1(b), we employ a 3-hidden-layer multilayer perceptron (MLP) with 512 hidden units for  $h_\theta$ . For training and test sets, we numerically sampled 1,000 positional trajectories in steady state for each model. Trajectories were sampled with time step  $\Delta\tau = 10^{-2}$ . The total number of steps  $L$  is  $10^4$ . We present the training results at  $T_c = 1$  in Fig. 2(b–e). Note that all reported results in Fig. 2 are from the test set. We also demonstrate NEEP estimation ability with various  $L$ ; see Supplemental Material IA for results.

For the  $N = 2$  case, as shown in Fig. 2(b), it is observed that our estimator provides accurate values not only for the ensemble average but also for a single trajectory over  $\tau$ . Here,  $S(\tau) \equiv \sum_{i=0}^{\tau/\Delta\tau} \Delta S(s_i, s_{i+1})$  and  $\sigma(\tau) \equiv \mathbb{E}[S(\tau)]$  where  $\Delta S$  is the analytic EP. Figure 2(c)

shows that the EP rate over the displacement space  $(x_1, x_2)$  calculated by NEEP (top panel) is same as the analytical solution (bottom panel). The local EP rate from NEEP at  $(x_1, x_2)$  is measured by averaging the EP rate produced when a particle passes through the point  $(x_1, x_2)$ .

To check the convergence of the training process, we plot the estimated values of  $\dot{\sigma}_\theta$  over training iteration in Fig. 2(d). The dashed red line indicates the analytic EP rate  $\dot{\sigma}$ . Insets in Fig. 2(d) are scatter plots between  $\Delta S_\theta$  and  $\Delta S$  in a randomly sampled single trajectory. As can be seen in the left inset, there is no correlation between  $\Delta S_\theta$  and  $\Delta S$  before training. But after training (right inset),  $\Delta S_\theta$  is well-fitted to  $\Delta S$  (coefficient of determination  $R^2 = 0.9972$ ).

As a high-dimensional task, we apply the same process for  $N = 5$ . In previous works [10, 13], estimating EP in a high-dimension system is extremely difficult because the methods have to obtain the empirical joint probability density. Here, despite the high-dimensionality of our given  $N = 5$  system,  $\Delta S_\theta$  is again well-fitted to  $\Delta S$  with  $R^2 = 0.9750$  (see Fig. 2(e)). Based on this result, NEEP can resolve the curse of dimensionality through a neural network. We also train our estimator at  $T_c = 2, 3, \dots, 10$  with  $T_h = 10$ , as shown in Fig. 2(a) with the estimated EP rate  $\dot{\sigma}_\theta$  plotted with symbols and error bars. Results show that NEEP accurately estimated the analytic value with small errors. Remarkably, these results are from the test set, implying that our approach can estimate EP even for unseen data.

Next, we demonstrate our method on the discrete flashing ratchet model [42], which consists of a particle moving in a one-dimensional periodic lattice. The particle drifts in a periodic asymmetric sawtooth potential, and the temperature of the heat bath is  $T$  (see Fig. 3(b)). For brevity, we set  $k_B = T = 1$ . Transition rates between each state  $s \in \{0, 1, 2, 0', 1', 2'\}$  are defined as  $k_{ij} = e^{(V_j - V_i)/2}$ ,  $k_{i'j'} = 1$ , and  $k_{ii'} = k_{i'i} = r$  where  $i, j \in \{0, 1, 2\}$ ,  $i', j' \in \{0', 1', 2'\}$ , and  $V$  is the potential that switches on and off at rate  $r$ . We set the switching rate  $r$  to 1. The EP per step is given as  $\dot{\sigma} = \sum_{\alpha, \beta} p(\alpha, \beta)(V_\alpha - V_\beta)$  [13].

We construct the NEEP as shown in Fig. 3(a) using word embedding [43], a method that transforms a discrete state into a trainable continuous vector called an embedding vector. We set the dimension of the embedding vector to 128 and employ a 2-hidden-layer MLP with 128 hidden units for  $h_\theta$ . From a set of different potential values, we sampled two single trajectories with  $L = 10^6$  steps for each potential  $V$ ; one trajectory is used for training and the other for testing. For the training data, we build five NEEPs, randomly initialized with

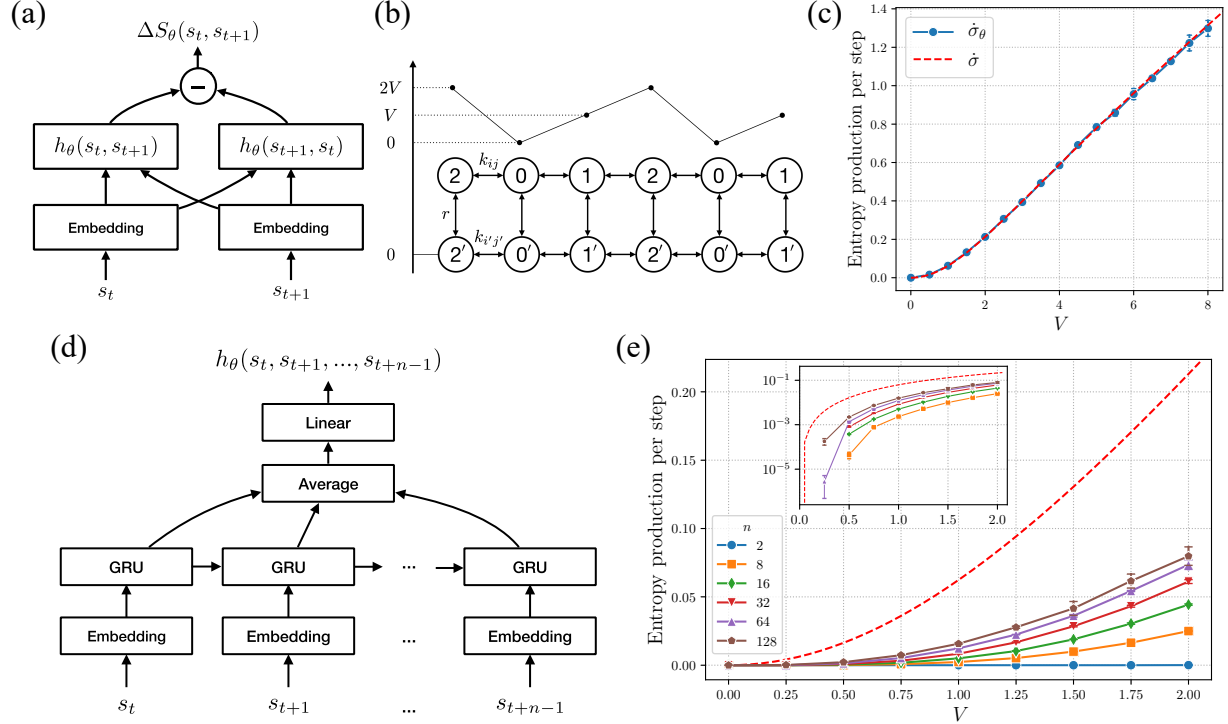


FIG. 3. (a) NEEP architecture for discrete state Markov chains. (b) Schematic of a discrete flashing ratchet model. (c) Entropy production per step as a function of potential  $V$ . The red dashed line is the analytic EP per step. (d) An RNN version of NEEP (RNEEP) for a non-Markovian process. (e) Results of RNEEP for a partial information problem. The inset shows a plot of the y-axis in log scale. Error bars represent the standard deviation of predictions from five independently trained estimators.

five different random seeds for each potential. Figure 3(c) shows that the analytical EP per step  $\dot{\sigma}$  is within the error bar of the NEEP predictions of  $\hat{\sigma}_\theta$ .

So far, we have tested Markovian systems, but of course most real-world time-series data are not Markovian. To test for non-Markovian application, we remove the on/off information from the states [13], i.e. states  $0'$ ,  $1'$ , and  $2'$  are not accessible. To address this partial information problem, we build  $h_\theta$  with a recurrent neural network (RNN). As shown in Fig. 3(d), we employ a gated recurrent unit (GRU) [44] with 128 hidden units. The RNN version of NEEP (RNEEP) takes input as a series of states with a sequence length of  $n$ , and the outputs of GRU are averaged over the sequence and then fed to a single layer feed-forward neural network. Now, the RNEEP output is defined as

$$\Delta S_\theta(\mathbf{s}_f) \equiv h_\theta(\mathbf{s}_f) - h_\theta(\mathbf{s}_r), \quad (8)$$

where

$$\mathbf{s}_f = (s_t, s_{t+1}, \dots, s_{t+n-1}),$$

$$\mathbf{s}_r = (s_{t+n-1}, \dots, s_{t+1}, s_t).$$

For each potential  $V$ , we train the RNEEP with six different sequence lengths  $n = 2, 8, 16, 32, 64$ , and  $128$ . As can be seen in Fig. 3(e), the RNEEP cannot detect any EP when  $n = 2$ , but with increasing sequence length  $n$ , the model prediction ( $\dot{\sigma}_\theta$ ) approaches the true value ( $\dot{\sigma}$ ). The inset in Fig. 3(e) shows that the RNN with sequence lengths of  $n = 64$  and  $n = 128$  can even detect EP at  $V = 0.25$ , where the EP is too tiny to be clearly observed. This result is meaningful because it shows that the RNEEP can distinguish between nonequilibrium and equilibrium states in the absence of measurable current [13, 14, 45]. See Supplemental Material I B for training details and convergence of the RNEEP.

In conclusion, we have developed a novel method, named NEEP, for estimating entropy production via neural networks. Our method does not require any prior knowledge of the system, but only trajectories. We proved that our method produces appropriate EP when the given system has a Markovian property and is in nonequilibrium steady state. We have demonstrated that NEEP precisely estimates the true EP of two nonequilibrium systems, namely bead-spring and discrete flashing ratchet models. In a continuous high-dimensional case, we verified that NEEP is free from the curse of dimensionality. Moreover, as a system without full description, we consider a non-Markovian model with partial information, with results showing that NEEP clearly distinguishes nonequilibrium and equilibrium states even for a small EP rate.

In previous approaches [1, 46], knowledge of the probability distribution and the irreversible current is essential to quantify how far the system is out of equilibrium. As NEEP does not require such detailed information, we expect our estimator to be applicable to various fields such as active matter, biological systems, electronic devices, and others. We further expect our method to be useful in distinguishing nonequilibrium states in the absence of observable currents, e.g. molecular motors with hidden internal states [45]. As a future work, modifying our NEEP method to estimate EP in more general nonequilibrium systems like time-dependent states will be intriguing research.

The code for NEEP, implemented in PyTorch [47], is available at <https://github.com/kdkyum/neep>.

## ACKNOWLEDGMENTS

This study was supported by the Basic Science Research Program through the National Research Foundation of Korea (NRF) (KR) [NRF-2017R1A2B3006930].

---

- [1] C. Battle, C. P. Broedersz, N. Fakhri, V. F. Geyer, J. Howard, C. F. Schmidt, and F. C. MacKintosh, *Science* **352**, 604 (2016).
- [2] S. C. Weber, A. J. Spakowitz, and J. A. Theriot, *Proc. Nat. Acad. Sci. U. S. A.* **109**, 7338 (2012).
- [3] C. Battle, C. M. Ott, D. T. Burnette, J. Lippincott-Schwartz, and C. F. Schmidt, *Proc. Nat. Acad. Sci. U. S. A.* **112**, 1410 (2015).
- [4] E. Ben-Isaac, Y. Park, G. Popescu, F. L. Brown, N. S. Gov, and Y. Shokef, *Phys. Rev. Lett.* **106**, 238103 (2011).
- [5] K. Sekimoto, *Stochastic energetics* (Springer-Verlag, 2010).
- [6] P. Martin, A. Hudspeth, and F. Jülicher, *Proc. Nat. Acad. Sci. U. S. A.* **98**, 14380 (2001).
- [7] T. Harada and S.-i. Sasa, *Phys. Rev. Lett.* **95**, 130602 (2005).
- [8] B. Lander, J. Mehl, V. Blickle, C. Bechinger, and U. Seifert, *Phys. Rev. E.* **86**, 030401 (2012).
- [9] F. Gnesotto, F. Mura, J. Gladrow, and C. Broedersz, *Rep. Prog. Phys.* **81**, 066601 (2018).
- [10] J. Li, J. M. Horowitz, T. R. Gingrich, and N. Fakhri, *Nat. Commun.* **10**, 1 (2019).
- [11] Q. Wang, S. R. Kulkarni, and S. Verdú, *IEEE Trans. Inf. Theory.* **51**, 3064 (2005).
- [12] R. Avinery, M. Kornreich, and R. Beck, *Phys. Rev. Lett.* **123**, 178102 (2019).
- [13] E. Roldán and J. M. R. Parrondo, *Phys. Rev. Lett.* **105**, 150607 (2010).
- [14] É. Roldán and J. M. Parrondo, *Phys. Rev. E.* **85**, 031129 (2012).
- [15] T. Van Vu, V. T. Vo, and Y. Hasegawa, arXiv:2001.07131 (2020).
- [16] S. Otsubo, S. Ito, A. Dechant, and T. Sagawa, arXiv:2001.07460 (2020).
- [17] R. Kawai, J. M. Parrondo, and C. Van den Broeck, *Phys. Rev. Lett.* **98**, 080602 (2007).
- [18] P. Mehta and D. J. Schwab, arXiv:1410.3831 (2014).
- [19] M. Koch-Janusz and Z. Ringel, *Nat. Phys.* **14**, 578 (2018).
- [20] S.-H. Li and L. Wang, *Phys. Rev. Lett.* **121**, 260601 (2018).
- [21] J. Carrasquilla and R. G. Melko, *Nat. Phys.* **13**, 431 (2017).

[22] E. P. Van Nieuwenburg, Y.-H. Liu, and S. D. Huber, *Nat. Phys.* **13**, 435 (2017).

[23] J. Venderley, V. Khemani, and E.-A. Kim, *Phys. Rev. Lett.* **120**, 257204 (2018).

[24] Y.-H. Liu and E. P. L. van Nieuwenburg, *Phys. Rev. Lett.* **120**, 176401 (2018).

[25] M. J. S. Beach, A. Golubeva, and R. G. Melko, *Phys. Rev. B* **97**, 045207 (2018).

[26] P. Zhang, H. Shen, and H. Zhai, *Phys. Rev. Lett.* **120**, 066401 (2018).

[27] G. Carleo and M. Troyer, *Science* **355**, 602 (2017).

[28] D.-L. Deng, X. Li, and S. Das Sarma, *Phys. Rev. X.* **7**, 021021 (2017).

[29] K. Ch'ng, J. Carrasquilla, R. G. Melko, and E. Khatami, *Phys. Rev. X.* **7**, 031038 (2017).

[30] K. Choo, G. Carleo, N. Regnault, and T. Neupert, *Phys. Rev. Lett.* **121**, 167204 (2018).

[31] G. Torlai, G. Mazzola, J. Carrasquilla, M. Troyer, R. Melko, and G. Carleo, *Nat. Phys.* **14**, 447 (2018).

[32] M. J. Hartmann and G. Carleo, *Phys. Rev. Lett.* **122**, 250502 (2019).

[33] A. Nagy and V. Savona, *Phys. Rev. Lett.* **122**, 250501 (2019).

[34] F. Vicentini, A. Biella, N. Regnault, and C. Ciuti, *Phys. Rev. Lett.* **122**, 250503 (2019).

[35] G. Carleo, I. Cirac, K. Cranmer, L. Daudet, M. Schuld, N. Tishby, L. Vogt-Maranto, and L. Zdeborová, *Rev. Mod. Phys.* **91**, 045002 (2019).

[36] N. Rahaman, S. Wolf, A. Goyal, R. Remme, and Y. Bengio, in *International Conference on Learning Representations* (2020).

[37] U. Seifert, *Rep. Prog. Phys.* **75**, 126001 (2012).

[38] Y. LeCun, Y. Bengio, and G. Hinton, *Nature (London)* **521**, 436 (2015).

[39] I. Goodfellow, Y. Bengio, and A. Courville, *Deep learning* (MIT press, 2016).

[40] F. Mura, G. Gradziuk, and C. P. Broedersz, *Phys. Rev. Lett.* **121**, 038002 (2018).

[41] F. S. Gnesotto, G. Gradziuk, P. Ronceray, and C. P. Broedersz, arXiv:2001.08642 (2020).

[42] A. Ajdari and J. Prost, *Comptes rendus de l'Académie des sciences. Série 2, Mécanique, Physique, Chimie, Sciences de l'univers, Sciences de la Terre* **315**, 1635 (1992).

[43] T. Mikolov, I. Sutskever, K. Chen, G. S. Corrado, and J. Dean, in *Advances in neural information processing systems* (2013) pp. 3111–3119.

[44] K. Cho, B. van Merriënboer, C. Gulcehre, D. Bahdanau, F. Bougares, H. Schwenk, and Y. Bengio, in *Proceedings of the 2014 Conference on Empirical Methods in Natural Language Processing (EMNLP)* (Association for Computational Linguistics, Doha, Qatar, 2014) pp. 1724–1734.

- [45] I. A. Martínez, G. Bisker, J. M. Horowitz, and J. M. Parrondo, *Nat. Commun.* **10**, 1 (2019).
- [46] J. Gladrow, N. Fakhri, F. MacKintosh, C. Schmidt, and C. Broedersz, *Phys. Rev. Lett.* **116**, 248301 (2016).
- [47] A. Paszke, S. Gross, F. Massa, A. Lerer, J. Bradbury, G. Chanan, T. Killeen, Z. Lin, N. Gimelshein, L. Antiga, A. Desmaison, A. Kopf, E. Yang, Z. DeVito, M. Raison, A. Tejani, S. Chilamkurthy, B. Steiner, L. Fang, J. Bai, and S. Chintala, in *Advances in Neural Information Processing Systems 32* (Curran Associates, Inc., 2019) pp. 8024–8035.
- [48] V. Nair and G. E. Hinton, in *Proceedings of the 27th international conference on machine learning (ICML-10)* (2010) pp. 807–814.
- [49] D. P. Kingma and J. Ba, arXiv:1412.6980 (2014).
- [50] U. Seifert, *Phys. Rev. Lett.* **95**, 040602 (2005).

## Supplemental Material: Learning entropy production via neural networks

### I. TRAINING DETAILS

We employ ReLU [48] as the activation function for the neural estimator for entropy production (NEEP). We train the estimators with the Adam [49] optimizer using the following hyper-parameters: learning rate 0.0001, weight decay 5e-5, and batch size 4096. We use these hyper-parameters for all processes unless noted. See Algorithm 1 for our training procedure. All runs were conducted on a single NVIDIA TITAN V GPU.

---

**Algorithm 1** Training the NEEP

---

**Require:** Model  $\Delta S_\theta$ , training set  $\{(s_1^i, s_2^i, \dots, s_L^i)\}_{i=1, \dots, M}$  where  $L$  is the trajectory length and  $M$  is the number of trajectories, optimizer

- 1: **loop**
- 2: Compute  $J(\theta) = \sum_{(i,t) \in \mathcal{B}} \Delta S_\theta(s_t^i, s_{t+1}^i) - e^{-\Delta S_\theta(s_t^i, s_{t+1}^i)}$  where  $\mathcal{B}$  is a randomly sampled subset of  $\{1, \dots, M\} \times \{1, \dots, L-1\}$  where  $\times$  is a Cartesian product. The total number of the sampled data points  $|\mathcal{B}|$  is equal to the batch size.
- 3: Compute gradients  $\nabla_\theta J(\theta)$ .
- 4: Update parameters  $\theta$  with the optimizer.
- 5: **end loop**

---

#### A. Bead-spring model

For the bead-spring model, we also check the prediction and training process of NEEP with respect to training set size  $L$ . With increasing trajectory length  $L$ , the prediction of NEEP is well converged to the true EP rate (see Fig. S1). Figure S2 shows NEEP prediction results with respect to training iteration for  $L = 2000, 5000, 10000$  and temperature  $T_c = 1, 5, 10$ . With 2 beads (see Fig. S2(a)), there is some overfitting [39] at  $L = 2000$ , but with increasing data size  $L$ , predictions from the training and test sets converge. With 5 beads, Fig. S2(b) shows that the prediction from the training set diverges at  $L = 2000$ , but strikingly, the prediction from the test set converges to the true EP rate. From this result,

we strongly recommend to divide the trajectories into training and test sets and see whether the prediction of the test set converges and not the prediction of the training set.

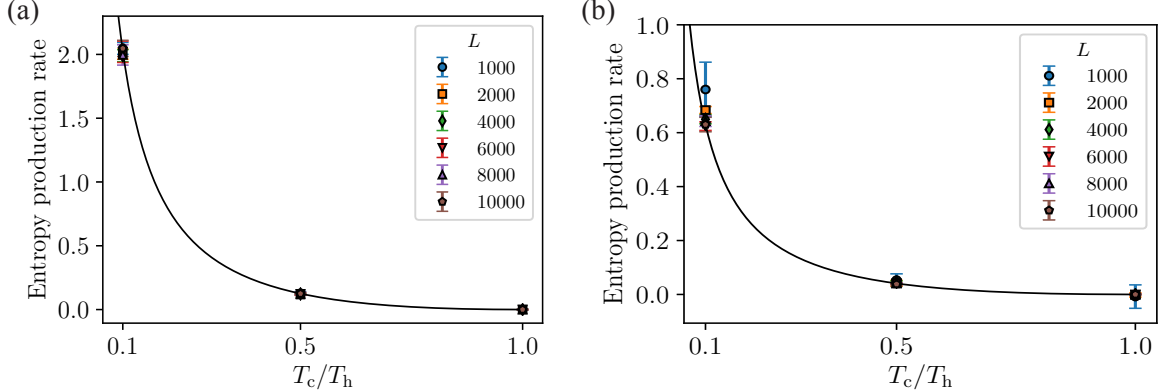


FIG. S1. Test set prediction of NEEP with  $L = 1000, 2000, 4000, 6000, 8000$ , and  $10000$  for the (a) 2-bead and (b) 5-bead models. The solid black line denotes the analytic EP rate. The error bar represents the standard deviation of estimations from five independently trained estimators.

## B. Discrete flashing ratchet

For the discrete flashing ratchet model, the number of training iterations is 50000. Note that these runs use a single trajectory, i.e.  $M = 1$  in Algorithm 1. As can be seen in Fig. S3, EP predictions per step converge to the true value (red dashed line). We train the RNEEP with a trajectory length of  $L = 5 \times 10^7$ , and the states  $0', 1',$  and  $2'$  are converted to  $0, 1$ , and  $2$ , respectively for the partial information problem. Figure S4 shows the results from RNEEP with sequence lengths  $n = 64$  and  $n = 128$  at potentials  $V = 1.25, 1.5, 1.75$ , and  $2.0$ . While some variation exists at  $n = 128$  and  $V = 2.0$ , the rest of the training dynamics converge.

## II. ANALYTIC DESCRIPTION

### A. Bead-spring model

The dynamics of the beads can be described by an overdamped Langevin equation given by

$$\dot{x}_i(\tau) = A_{ij}x_j(\tau) + \sqrt{2T_i/\gamma}\xi_i(\tau), \quad (\text{S1})$$

where  $A_{ij} = -2k/\gamma \delta_{i,j} + k/\gamma (\delta_{i,j+1} + \delta_{i+1,j})$ ,  $\mathbf{x} = (x_1(\tau), x_2(\tau), \dots, x_N(\tau))$ ,  $\boldsymbol{\xi} = (\xi_1(\tau), \xi_2(\tau), \dots, \xi_N(\tau))$  and the temperature  $T_i$  of each heat bath linearly varies from  $T_c$  to  $T_h$ . These different temperatures induce a thermodynamic force which drives the system out of equilibrium. Here,  $\gamma$  is the Stokes friction coefficient, and  $\boldsymbol{\xi}$  is an independent Gaussian white noise vector satisfying  $\mathbb{E}[\xi_i(t)\xi_j(t')] = \delta_{ij}\delta(t-t')$ . For brevity, we set  $k_B = 1$ . To calculate the entropy production (EP) of the  $N = 2$  bead-spring model, we have to consider the Fokker-Planck equation given by

$$\frac{\partial p(\mathbf{x}, \tau)}{\partial \tau} = -\nabla_{\mathbf{x}} \cdot \mathbf{j}_{\mathbf{x}}(\mathbf{x}, \tau), \quad (\text{S2})$$

where the probability current  $\mathbf{j}_{\mathbf{x}}(\mathbf{x}, \tau)$  is defined by

$$\mathbf{j}_{\mathbf{x}}(\mathbf{x}, \tau) = \mathbf{A}\mathbf{x}p(\mathbf{x}, \tau) + \mathbf{D}\nabla_{\mathbf{x}}p(\mathbf{x}, \tau). \quad (\text{S3})$$

Here, the deterministic term  $\mathbf{A} \equiv \frac{k}{\gamma} \begin{pmatrix} -2 & 1 \\ 1 & -2 \end{pmatrix}$  and the diffusion term  $\mathbf{D} \equiv \frac{1}{\gamma} \begin{pmatrix} T_1 & 0 \\ 0 & T_2 \end{pmatrix}$ . Since the steady state probability density function is Gaussian as  $p_{st} \propto \exp[-(1/2)\mathbf{x}^T \mathbf{C}^{-1} \mathbf{x}]$  with a covariance matrix  $\mathbf{C}$ , the solution can be derived by the Lyapunov equation

$$\mathbf{AC} + \mathbf{CA}^T = -2\mathbf{D}, \quad (\text{S4})$$

so the covariance matrix is given by

$$\mathbf{C} = \frac{1}{12k} \begin{pmatrix} 7T_h + T_c & 2(T_h + T_c) \\ 2(T_h + T_c) & T_h + 7T_c \end{pmatrix}. \quad (\text{S5})$$

Using Eq. (S5), the probability density function and the probability current in steady state,  $p(\mathbf{x})$  and  $j_{ss}(\mathbf{x})$ , can be obtained.

The EP rate along a trajectory is given by [50]

$$\begin{aligned} \dot{S}(\tau) &= \dot{S}_m(\tau) + \dot{S}_s(\tau) \\ &= -\frac{\partial \tau p(\mathbf{x}, \tau)}{p(\mathbf{x}, \tau)} \Big|_{\mathbf{x}(\tau)} + \frac{\mathbf{j}(\mathbf{x}, \tau)^T \mathbf{D}^{-1}}{p(\mathbf{x}, \tau)} \Big|_{\mathbf{x}(\tau)} \dot{\mathbf{x}}, \end{aligned} \quad (\text{S6})$$

where  $\dot{S}_m(\tau)$  is the entropy rate from the heat dissipated into the environment and  $\dot{S}_s(\tau)$  is for the system. Because the first term on the right-hand side vanishes in steady state, the ensemble averaged entropy production rate is obtained by

$$\dot{\sigma} = \int d\mathbf{x} \frac{\mathbf{j}_{ss}(\mathbf{x})^T \mathbf{D}^{-1}}{p(\mathbf{x})} \mathbf{j}_{ss}(\mathbf{x}). \quad (\text{S7})$$

Inserting the solutions from Eq. (S2) and Eq. (S3), the EP rate is obtained by

$$\dot{\sigma} = \frac{k(T_h - T_c)^2}{4\gamma T_h T_c}. \quad (\text{S8})$$

In the same way, the EP rate for the  $N = 5$  bead-spring model can be obtained as

$$\dot{\sigma} = \frac{k(T_h - T_c)^2(111T_h^2 + 430T_hT_c + 111T_c^2)}{495\gamma T_h T_c (3T_h + T_c)(T_h + 3T_c)}. \quad (\text{S9})$$

We analytically calculated the local EP rate in Fig 2(c) (bottom) using the integrand of Eq. (S7). Because our NEEP model estimates along the time evolution of a particle, the local EP rate from NEEP  $\sigma_\theta(\mathbf{x})$  is measured by the following equation:

$$\dot{\sigma}_\theta(\mathbf{x}) = \frac{1}{L\Delta\tau} \sum_{i=0}^L \delta(\mathbf{x} - \mathbf{x}_i^m) \Delta S_\theta(\mathbf{x}_i, \mathbf{x}_{i+1}), \quad (\text{S10})$$

where  $\Delta\tau$  is time step of a trajectory  $\mathbf{x}_1, \dots, \mathbf{x}_L$  and  $\mathbf{x}_i^m = (\mathbf{x}_i + \mathbf{x}_{i+1})/2$ .

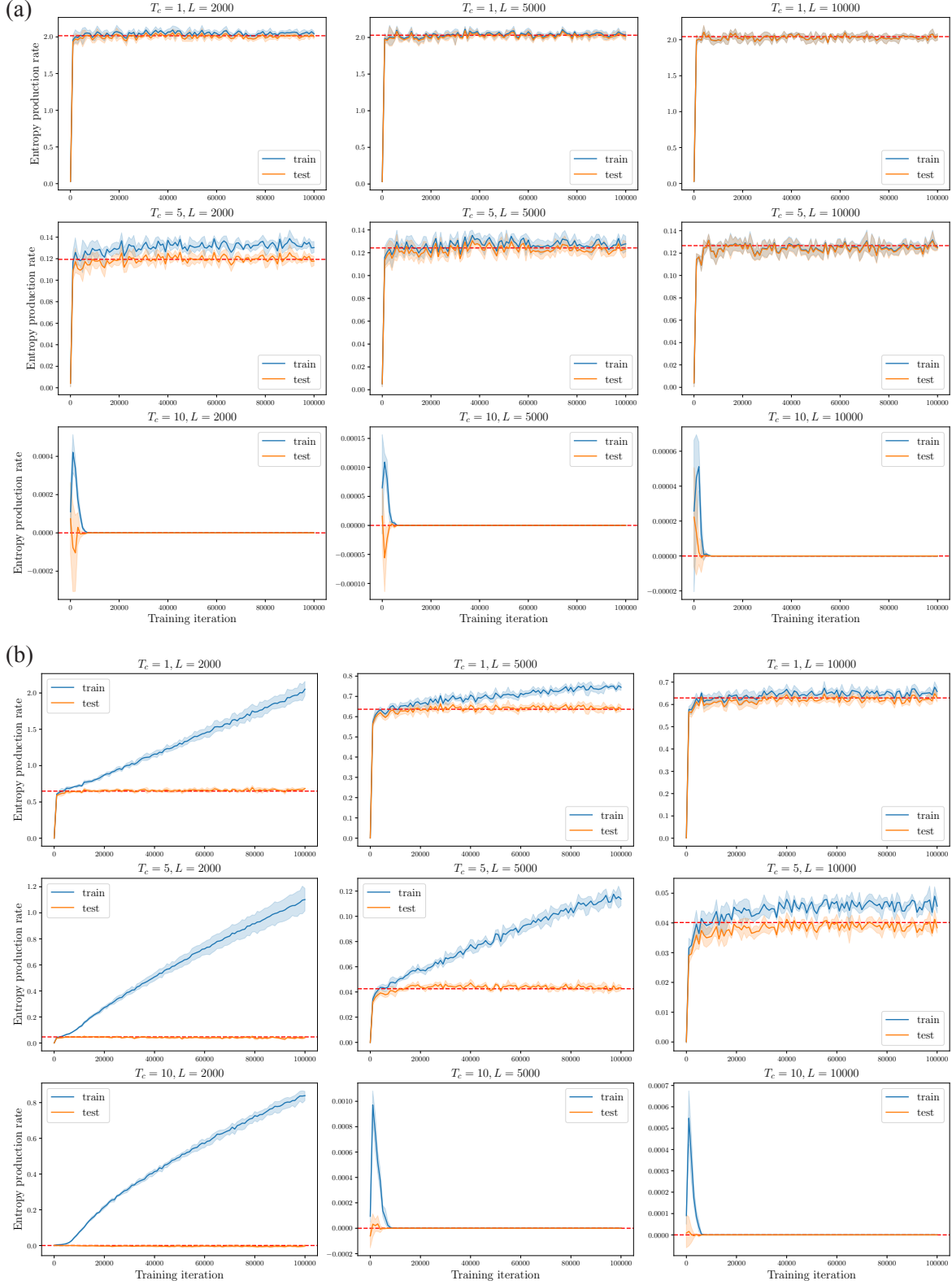


FIG. S2. Training process of NEEP for  $L = 2000, 5000, 10000$  and corresponding  $T_c = 1, 5, 10$  for the (a) 2-bead and (b) 5-bead models. The red dashed line represents the analytic EP rate.

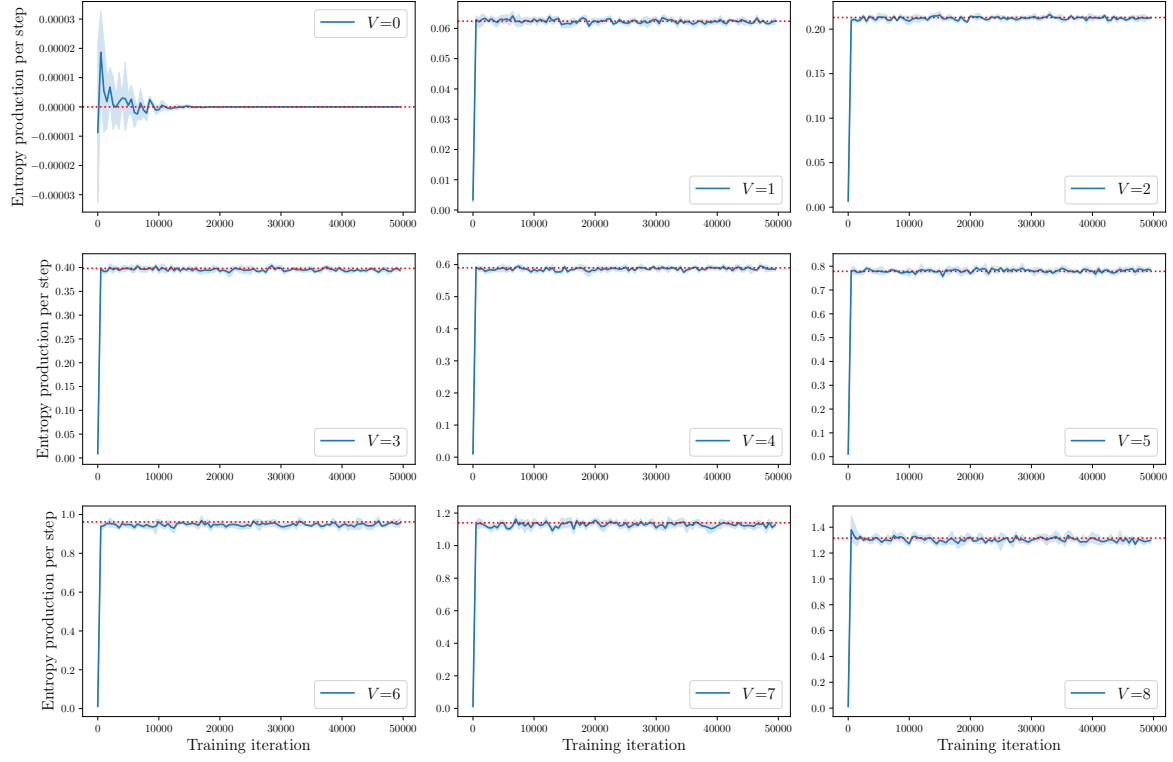


FIG. S3. Predictions of EP per step over training iteration with respect to nine different potential  $V$ .

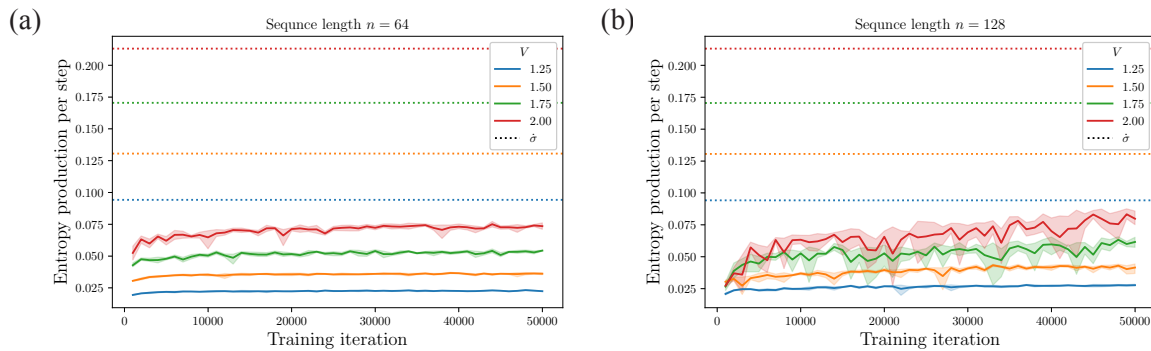


FIG. S4. Predictions of EP per step over training iteration by the RNEEP for (a)  $n = 64$  and (b)  $n = 128$ .